LATITUDINAL DISTRIBUTION OF NIGHTTIME AURORAL PRECIPITATION DURING MAGNETIC CALM AND NEAR THE TIME OF SUBSTORM ONSET

© 2025 V.G. Vorobjev[1], O.I. Yagodkina[1], E.E. Antonova[2,3], I. P. Kirpichev[3]

[1]Polar Geophysical Institute, Apatity, Murmansk Region, Russia
[2]Skobeltsyn Institute of Nuclear Physics, Moscow State University, Moscow, Russia
[3]Space Research Institute Russian Academy of Science, Moscow, Russia

**e-mail: vorobjev@pgia.ru*
***e-mail: oksana41@mail.ru*
****e-mail: elizaveta.antonova@gmail.com*
*****e-mail: ikir@iki.rssi.ru*

Received May 19, 2024

Revised September 06, 2024

Accepted September 26, 2024

Abstract. The unresolved problems of the physics of auroral substorms include the issue of localization and the mechanism of the start of the substorm expansion phase. The new information needed to solve this problem can be obtained by comparing the results of observations from low-altitude spacecraft with observations in the equatorial plane of the magnetosphere. For this purpose, the morphological projection method was used, which does not require knowledge about the configuration of the magnetic field. This paper considers the latitudinal profiles of the auroral precipitation characteristics at ionospheric altitudes obtained from DMSP F7 spacecraft observations and the radial distribution of ion pressure in the equatorial plane according to the THEMIS mission during periods of magnetic calm and at time intervals close to the auroral breakup. Special attention was paid to the position of the maximum energy flux of the precipitation of ions with energy larger than 3 keV and ion pressure profiles. The average ion pressure latitudinal profiles at low altitudes were determined and compared with the average pressure distributions in the equatorial plane of the magnetosphere under similar to averaged values of solar wind and geomagnetic activity parameters. It is shown that, if under geomagnetic calm the pressure maximum at low altitudes is mapped to geocentric distances of ~7−8 Re, before the substorm onset it is mapped to a distance of ~5−6 Re. The averaged values of the pressure maxima during the magnetic calm, as well as before and after substorm onset were obtained. The brightness of the auroral luminosity in the 557.7 nm emission was estimated from DMSP F7 observations of the average energy and energy flux of the precipitated electrons.

DOI: 10.31857/S00167940250201e9

1. INTRODUCTION

Early studies of magnetospheric substorms showed that the brightening of the auroral arc closest to the equator indicates the localization of the onset of the substorm expansion phase [Akasofu, 1964]. Such substorms are usually called classical in contrast to , for example, substorm disturbances developing at latitudes above 70° geomagnetic latitude, which are called "polar substorms" [Kleimenova et al., 2012; Despirak et al., 2022]. Attention to the question of localizing the onset of the substorm expansion phase has increased in connection with studies of electron acceleration in the outer radiation belt, as substorm electron injections are considered the seed population for electron acceleration in the outer radiation belt. For a long time, it was believed that the injected seed electrons were then accelerated to relativistic energies over a comparatively long period. However, a detailed analysis in [Kim et al., 2023] showed that the main mechanism for accelerating electrons in the outer belt is substorm dipolarization. It was previously shown that dispersionless injections can be localized inside the geostationary orbit (see, for example, [Nosé et al., 2016, 2018]). There arose a need to clarify the localization and mechanisms of the onset of the expansion phase of a classical substorm. In [Vorobjev et al., 2018], it was shown that during substorms with relatively large minimum values of the *AL* -index (− 1500 nT < *AL* min < − 600 nT), an almost linear dependence of *SYM/H* on the modulus of *AL* (Fig. 1 *of* this paper) is clearly distinguished, which indicates the localization of the substorm disturbance inside the ring current. It is well known that the development of the ring current is a consequence of increased plasma pressure inside the magnetosphere. Therefore, observations of the dynamics of the radial plasma pressure profile in the magnetosphere during the preparatory phase of a substorm and a more detailed study of the localization of the expansion phase onset are of interest.

In the present work, an analysis of characteristics of nighttime auroral precipitation obtained by low-altitude polar-orbiting satellite DMSP F7 is conducted, and the results of pressure distribution analysis are compared with observations near the equatorial plane of the magnetosphere based on THEMIS mission data. The obtained statistics of auroral oval crossings by the DMSP satellite do not yet allow for identification of crossing moments of precipitation regions during the auroral breakup period. Even on satellites with increased temporal resolution , such as Fast and Frejia , each such event is a subject of separate special analysis [Persson et al., 1994; Dubyagin et al., 2003; Mende et al., 2003]. However, observations far from the equatorial plane were extremely

difficult to use for localizing the onset of the explosive phase of a substorm, as the popular magnetic field models with fixed geometry of current systems developed by that time did not allow for relatively accurate tracking of the magnetic field configuration. Mainly, there were competing theories of the explosive phase onset in the tail at a geocentric distance of ~20 Re as a result of reconnection processes [Baker et al., 1996] and the disruption of the tail current sheet at a distance of ~8−10 Re [Lui et al., 1996]. Magnetic field models were used to project observations from low-flying satellites. In the work [Dubyagin et al., 2003] the location of the substorm explosive phase onset region was determined at a geocentric distance of ~8 Re, which significantly supported the concept of substorm initiation within the magnetosphere. This result was obtained using the T-89 model [Tsyganenko, 1989]. This work also used the assumption of pressure isotropy p and measurement results of the proton flux maximum position, considered as the boundary of isotropic precipitation $b\ 2\ i$. An estimate of pressure magnitude in the breakup region of ~1−2 nPa was obtained by calculating the radial component of the Ampere force, equal to $\nabla p = [\mathbf{jB}]$, into the magnetosphere, starting from X=−25 Re in the neutral sheet at the midnight meridian. The integral plasma pressure, reconstructed from Fast satellite data, which measured ion fluxes with energies of 0.01−24 keV (see the top panel in Fig. 4 of that work), was at maximum ~0.4−0.5 nPa, which was significantly less than the pressure , reconstructed using the T-89 model [Tsyganenko, 1989]. The position of the pressure maximum coincided with the position obtained using the model, which was considered as validation of the breakup localization estimate at a geocentric distance of ~8 Re. It can be noted that the smaller magnitude of pressure determined from satellite data compared to calculation results is apparently related to the existence of a field-aligned potential of the order of several keV in an inverted-V type structure (see the top panel of Fig. 3 of the same work). Direct measurements of pressure in the equatorial plane of the magnetosphere and measurements of the pitch-angle distribution of electrons during the brightening of the aurora arc at the moment of breakup were not conducted in [Dubyagin et al., 2003]. But this work can be considered one of the first to draw attention to the use of pressure on the magnetic field line as a method for determining the projection of low-altitude measurements onto the equatorial plane.

Pitch-angle distribution measurements at the time of the breakup according to Fast satellite data were presented in [Mende et al., 2003] and corresponded to the results obtained in [Dubyagin et al., 2003] for similar invariant latitudes. It was shown that at the moment of breakup, the satellite registered a collimated electron beam at the boundary of an inverted V-type structure. This feature was not described by popular models of the substorm explosive phase onset, but may be important

for resolving the question of whether isolated substorms coincide with or differ significantly from substorms during a magnetic storm.

Later, detailed measurements of ion pressure near the equatorial plane of the magnetosphere appeared, which made it possible to show that the main part of the auroral oval projects not onto the plasma sheet, but onto the plasma ring surrounding the Earth, in which the high-latitude part of the ring current flows (see review [Antonova et al., 2018]). The obtained results allow for comparisons of pressure distribution at ionospheric heights and in the equatorial plane of the magnetosphere when analyzing substorms.

The latitudinal distribution of precipitating electron and ion fluxes in the auroral zone is extremely variable and depends on both the state of the interplanetary medium and the disturbance level of the magnetosphere and ionosphere. Averaged characteristics of auroral precipitation based on DMSP data, despite certain difficulties in selecting passes for such analysis, can provide some insight into the features of the latitudinal distribution of precipitation in various geophysical situations. To obtain average precipitation characteristics, it is necessary to identify a certain special or reference feature of precipitation that could be determined in each satellite crossing of the auroral zone, and relative to which it would be physically reasonable to determine precipitation characteristics. Such a reference point on the latitudinal precipitation profile can be the latitude of the boundary, named in [Newell et al., 1996] boundary $b\,2\,i$, where the maximum flux of precipitating ions with energy >3 keV is observed. The position of the $b\,2\,i$ boundary near midnight closely coincides (correlation coefficient $r = 0.92$) with the position of the ion isotropization boundary (IB) for ions with energy ~30 keV [Newell et al., 1998]. The isotropization boundary is believed to characterize the stretching of magnetic field lines in the nightside magnetosphere in the antisunward direction. Such stretching is usually associated with the growth of cross-tail currents during the substorm growth phase, but it can also be caused by the growth of the partial ring current (see the abstract of [Newell et al., 1998]).

In the literature (see, for example, [Vorobjev et al., 2003]), the term "isotropization boundary" is often used instead of the boundary $b\,2\,i$, which can lead to some misunderstanding. The position of the isotropic precipitation boundary due to non-conservation of the particle's magnetic moment can only be considered in a single-particle model of particle motion in a laminar magnetic field. It is determined by the particle energy and the ratio of the particle's Larmor radius to the scale of magnetic field inhomogeneity. Therefore, despite numerous studies on determining the boundaries of isotropic precipitation of particles of different energies, such boundaries cannot be effectively used to determine the localization of auroral breakup. The boundary $b\,2\,i$ was determined by the

flux of precipitating ions (all ions were considered protons, which is applicable mainly to magnetically quiet conditions) with energies >3 keV, which is close to ion pressure if the average ion energy is large compared to the selected threshold. The results of Vorobjev et al. [2003] showed the effectiveness of using $b\ 2\ i$ in the analysis of substorm dynamics. Therefore, in this work, we consider the position of the boundary $b\ 2\ i$ as an effective method for studying the dynamics of auroral precipitation.

Auroral precipitations registered by DMSP satellites at latitudes higher than $b\ 2\ i$, are characterized as isotropic. Under conditions of magnetostatic equilibrium in isotropic plasma, its characteristics (pressure, temperature, and density) remain constant along the geomagnetic field line [Goertz and Baumjohann, 1991] in regions where the ion temperature greatly exceeds the longitudinal potential difference. Thus, on one hand, as is usually done, characteristics of magnetospheric plasma can be obtained by projecting data collected at ionospheric altitudes onto the equatorial plane of the magnetosphere using some magnetic field model. On the other hand, the condition of equality of ion characteristics in the ionosphere and magnetosphere allows projecting latitudinal profiles of auroral precipitations, obtained at ionospheric altitudes, onto the equatorial plane of the magnetosphere without using any magnetic field models by the method of "morphological projection" according to the classification [Paschmann et al., 2002].

The purpose of this work is to study the latitudinal distribution of characteristics of nighttime auroral precipitations during quiet periods and during the onset of magnetospheric substorms, to study the spatial distribution and dynamics of proton and electron precipitations during the substorm growth phase, and to determine the localization area of auroral breakup in the equatorial plane of the magnetosphere using the "morphological projection" method.

2. DATA AND METHODOLOGY

For the analysis of auroral precipitation characteristics, data from the DMSP F7 satellite in the 3-hour interval 21:00−24:00 MLT were used. The satellite had an almost circular polar orbit with an altitude of ~835 km and an orbital period of ~101 min. Every second, the satellite recorded the spectrum of precipitating particles in the energy range from 32 eV to 30 keV across 19 channels, distributed by energy in a logarithmic sequence. Corrected geomagnetic coordinates (CGL, MLT) of the satellite trajectory at an altitude of 110 km were calculated using the AACGM model [Baker and Wing, 1989]. Satellite data were taken from the pages (http://sd-www.jhuapl.edu).

As the primary material in the work, we used the DMSP satellite database F7 for 1986, created and presented earlier in the work [Vorobjev et al., 2003]. In addition to the characteristics of precipitating particles and information on the level of magnetic activity, the database for each satellite passage through the auroral precipitation zone contains information about the phases of magnetic substorms necessary for the purposes of this study. The database identifies four phases of substorm activity: (1) magnetically quiet period, (2) growth phase, (3) expansion phase, and (4) recovery phase. Each of phases 2, 3, and 4 is additionally divided into three equal time interval subphases corresponding to the initial, middle, and final stages of each phase.

The DMSP satellite database contains more than 32,000 satellite crossings of the auroral zone. The phases of magnetic disturbance for this database were determined by visual analysis of diurnal variations of the *AL* -index. Such methodology is quite acceptable for statistical processing of large data arrays. However, for the present study, a more detailed analysis of the level of magnetic disturbance is necessary. For this purpose, for each individual satellite crossing of the auroral zone selected from the corresponding category of the database, the state of geomagnetic activity and phases of the magnetospheric substorm were additionally determined by detailed analysis of 1-minute values of the *AL* -, *SYM/H* - and *PC-indices* of magnetic activity. Variations of the *Bz* - component of the IMF and the solar wind dynamic pressure *Psw* were also used when corresponding data were available on the OMNI Web pages (http://cdaweb.gsfc.nasa.gov/).

When analyzing the characteristics of auroral particles using data from the F7 satellite, besides their average energies and energy fluxes, ion pressure values (*Pi*) were used for precipitating ions, and for precipitating electrons, I_{5577} - the emission intensity in the (OI) 557.7 nm emission. The methodology for determining ion pressure from DMSP satellite measurements was first published in the paper [Wing and Newell, 1998]. In the present work, a modified version of this methodology is used, proposed in the work [Stepanova et al., 2006], which allows obtaining pressure values above the region of electron field-aligned acceleration and making comparisons with pressure near the equatorial plane. Ion pressure is calculated assuming a Maxwellian energy distribution of particles. Despite the fact that non-Maxwellian energetic tails of distribution functions are often registered in the auroral zone [Wing and Newell, 1998], this does not lead to significant errors in pressure calculations in the considered regions, as the κ index of the ion function when approximated by a kappa distribution is ~10 [Kirpichev et al., 2021].

The algorithm for calculating the integral emission intensity of (OI) 557.7 nm is presented in the work [Vorobyev et al., 2013]. When calculating the emission intensity, the processes of formation of the electronically excited oxygen atom O(^{1}S) as a result of energy transfer from the

metastable state $N_2(A\,^3\Sigma_u^+)$, excitation of $O(^3P)$ by primary and secondary electrons, and dissociative recombination were taken into account. The average energy and integral energy flux of precipitating electrons were used as input parameters for the model, which could sometimes lead to underestimation of the emission level in regions of narrow electron beams whose crossing time by the satellite is less than the spectrometer's temporal resolution, i.e., those with a thickness of less than ~7-8 km. Such beams are formed as a result of acceleration of electrons of ionospheric origin along magnetic field lines (see discussion in [Vorobjev et al., 2024]).

In the work of [Roach and Jamnick, 1958], it was established that the faintest glow that the human eye can distinguish in the night sky must be 3-4 times more intense than the normal glow of the night sky. The brightness of auroral glow is measured in kiloRayleighs (kR). If we assume that the glow level of a clear night sky in the 557.7 nm emission is approximately 0.15-0.20 kR, then the human eye, adapted to the level of night sky glow, can distinguish an aurora with an intensity in the green line of more than ~0.6-0.8 kR. According to the international classification, depending on the brightness of the 557.7 nm emission, auroras are divided into 4 classes. The first class consists of weak auroras up to 1 kR, with brightness comparable to that of the Milky Way. The second class includes medium intensity auroras up to 10 kR, comparable in brightness to cirrus clouds illuminated by the Moon. The third class comprises bright auroras up to 100 kR, comparable in brightness to cumulus clouds illuminated by the Moon. The fourth class includes very bright auroras with a glow intensity of up to 1000 kR. Such auroras create illumination on the Earth's surface comparable to that from a full Moon.

Section 5 of this paper compares the latitudinal profiles of ion pressure obtained from observations of the F7 satellite with the radial distribution of *Pi* in the equatorial plane of the magnetosphere according to data from THEMIS mission satellites, published on the website (https://themis.ssl.berkeley.edu/data/themis/) . Measurements by the DMSP F7 satellite were conducted in 1986 - a year of quiet Sun in the minimum of the 21st solar activity cycle. Data from THEMIS satellites were used for 2008-2010 during the minimum of the 23rd solar activity cycle, so there should not be a large difference in the position of the *b* 2 *i* boundary depending on the phase of the solar cycle.

3. DETERMINATION OF CHARACTERISTICS OF NIGHTTIME AURORAL PRECIPITATIONS DURING MAGNETICALLY QUIET PERIODS

Quiet periods included satellite passes observed during low magnetic activity ($AL > -100$ nT) and in the absence of magnetic variations with amplitudes greater than 50 nT in a time interval of approximately 2 hours before and after the satellite recorded precipitations in the auroral zone. Such detailed analysis allows separating "truly" magnetically quiet periods from intervals with low magnetic activity that belong to the substorm initiation phase or to intervals of insignificant growth in magnetic activity caused by short-term southward turns of the *Bz* component of the IMF (*DP2* variations).

Fig.1.

A typical example of one such event is presented in Fig. 1, which shows interplanetary medium parameters and magnetic activity indices in the interval 01:00-05:00 UT on October 8, 1986. The time of the satellite pass is indicated by a vertical dashed line. The satellite pass was observed during a period of very low magnetic activity with a northward orientation of the IMF. The values of the *PC* index were close to zero, and the magnitude of the *AL* index even at peak values was not lower than − 20 nT.

Fig.2.

Latitudinal distributions of characteristics of ion (*a*) and electron (*b*) precipitations observed by the F7 satellite during this pass are presented in Fig. 2. From top to bottom in Fig. 2 *a* are shown the average energies (*Ei* , keV) and energy fluxes (*Fi* , erg/cm ^{2}s) of ion precipitations, and in Fig. 2 *b* - the average energies (*Ee* , keV) and energy fluxes (*Fe* , erg/cm ^{2}s) of electron precipitations. The dots on the graphs correspond to the values of parameters measured by the satellite. The corrected geomagnetic latitude (CGL) is plotted along the horizontal axis. In this satellite pass, the position of the maximum *Fi* , corresponding to the position of the boundary *b* 2 *i* was recorded at latitude 67.8° CGL at 03:09 UT (time rounded to minutes). In Fig. 2, the position of *b* 2 *i* is marked by a vertical dashed line.

Fig.3.

For this satellite pass, the latitudinal profile of ion pressure (*Pi*) is presented in Fig. 3 *a* . Ion pressure is determined by the energy flux of precipitating ions and their average energy. The average energy of precipitating ions in the auroral precipitation region changes insignificantly, therefore the latitudinal profile of ion pressure is similar to the latitudinal profile of *Fi* , and the maximum of *Pi* approximately coincides with the position of the boundary *b* 2 *i* . In Fig. 3 *a* , the latitude of the ion pressure maximum with a value of ~0.4 nPa coincides with the position of *b* 2 *i* and is marked by a vertical dashed line. When calculating the pressure , as well as when calculating the average energies and energy fluxes of ions , the existence of a field-aligned potential drop was

not taken into account. The region of low (~0.2 nPa) pressure poleward of the maximum apparently corresponds to an inverted-V type structure with a characteristic energy of ~3 keV, blocking the precipitation of ions with energies not exceeding this value. In the region of relatively high pressure values, the field-aligned potential difference is small, which can be seen when comparing Figures 2 and 3, and therefore, the calculated pressure values are close to the pressure in the equatorial plane.

Equatorward of *b* 2 *i* , the ion pressure decreases rapidly due to the decrease in the parallel component of *Pi* and the rapid growth of its perpendicular component. Poleward of *b* 2 *i* , overall, a more gradual decrease in ion pressure is observed.

The intensity of the 557.7 nm emission for this satellite pass is shown in Fig. 3 *b* . The value of I_{5577} is determined mainly by *Ee* and *Fe.* The value of the average energy of precipitating electrons in the energy range of 1-10 keV weakly affects the emission level of 557.7 nm, therefore, as in the case of the ion population, the latitudinal variation of the emission approximately corresponds to the latitudinal distribution of the energy flux of precipitating electrons. According to Fig. 2 *b* and 3 *b,* electron precipitation even in such an "extremely" quiet period is recorded from the boundary *b* 2 *i* at latitude 67.8° CGL to approximately 71° CGL. The luminosity during this period can be attributed to subvisual or very weak auroras, excluding the sharp local increase in the energy flux of precipitating electrons at latitudes 70.8°-71.0° CGL, which is most likely associated with an aurora arc with an intensity of about 4 kR.

Fig. 4.

The average latitudinal distribution of ion pressure during quiet periods is shown in Fig. 4 *a* . The curve was obtained by the superposed epoch method relative to *b* 2 *i* , the average latitude of which during quiet periods is $\Phi' = 68.3° \pm 0.6°$ CGL and is indicated by a vertical dashed line. The average values of magnetic activity indices and interplanetary medium parameters during satellite passes indicate a very low level of geomagnetic activity: $< AL >= -12$ nT, $< Dst >= -2$ nT, <IMF *Bz* > = +2.3 nT and $< Psw >= 2.5$ nPa. The latitudinal distribution of ion pressure in Fig. 4 *a* was obtained by averaging data from 20 satellite passes through the precipitation zone. Increasing the number of satellite passes to obtain average characteristics does not lead to significant changes in the ion pressure profile. However, in the region of discrete electron precipitation, it leads to strong smoothing of the energy fluxes of precipitating electrons and, consequently, to a decrease in the average luminosity values.

4. CHARACTERISTICS OF AURORAL PRECIPITATIONS DURING THE PERIODS BEFORE AND AFTER THE ONSET OF THE SUBSTORM EXPANSION PHASE

The average distribution of ion pressure in the final stage of the substorm growth phase, approximately in the interval of 15 minutes before the onset of the expansion phase (T_0) is shown in Fig. 4 *b* . For this study, satellite passes with a well-defined substorm growth phase in the *AL* and *PC* indices and a clearly defined moment *T* 0 *in the* $_{AL}$ index were selected. The latitudinal distribution of ion pressure in Fig. 4 *b* was obtained by averaging data from 18 satellite passes through the precipitation zone. The average parameters of magnetic activity and interplanetary medium in these satellite passes are: < *AL* >= − 65 nT, < *Bz* IMF>= − 1.4 nT, < *Psw* >= 3.3 nPa . Figure 4 *b* shows that in relation to magnetically quiet conditions, during the substorm growth phase, the boundary *b* 2 *i* shifted toward the equator and just before the onset of the expansion phase, on average, is located at the latitude Φ′= 65.4° ± 0.7° CGL . The value of ion pressure at *b* 2 *i* increases from < *Pi* > = (0.6 ± 0.1) nPa during quiet periods (Fig. 4 *a*) to < *Pi* > = (1.1 ± 0.1) nPa in the final stage of the growth phase.

The average distribution of ion pressure in the initial period of the substorm expansion phase is illustrated in Fig. 4 *c* . Averaging was done over 16 passes of F7, which occurred in the first third of the total period of the substorm expansion phase, corresponding to an interval of ~15 min, taking into account that the moment T_0 itself is determined from magnetic data with an accuracy of several minutes. The figure demonstrates that the latitudinal position of the boundary *b* 2 *i* before and after the beginning of the substorm expansion phase practically did not change and equals Φ′= 65.4° ± 0.7° CGL, but the magnitude of ion pressure decreased to < *Pi* > = (0.8 ± 0.1) nPa, possibly due to an increase in field-aligned current after the beginning of the substorm expansion phase, leading to an increase in the field-aligned potential difference, growth of electron precipitation, and inhibition of ion precipitation.

Fig. 5.

Latitudinal characteristics of electron precipitation are presented in Fig. 5 *a* − *c* . Panels *a* − *c* of Fig. 5 show average latitudinal profiles of 557.7 nm emission luminosity, obtained from observations of average energies and energy fluxes of precipitating electrons in the corresponding satellite F7 passes shown in Fig. 4 *a* − *c* . Overall, Fig. 5 *a* − *c* shows that the main electron precipitation is registered in the region of isotropic precipitation poleward of *b* 2 *i* . Equatorward of *b* 2 *i* before the beginning of the substorm expansion phase (Fig. 5 *a* and 5 *b*), there exists a very narrow ~0.5° latitude region of weak subvisual diffuse luminosity. After the beginning of the substorm expansion phase, the brightness of luminosity equatorward of *b* 2 *i* increases to 4−8 kR, and the width of the luminosity region increases to ~2° latitude.

During quiet periods (Fig. 5 *a*), weak subvisual glow is observed poleward of *b* 2 *i* up to ~70° CGL. A noticeable increase in emission intensity is observed at latitudes 70°−72° CGL. In this latitude range, virtually every satellite pass records 1 to 3 sharp local increases in emission intensity, often up to several tens of kR, which are most likely associated with the quiet auroral oval arcs. An example of such a local increase in emission intensity during the satellite pass on October 08, 1986 is shown in Fig. 3 *b* . Averaging data across all events gives a smoothed picture in this region of discrete precipitation, which is presented in Fig. 5 *a* . Increasing the number of satellite passes to obtain average characteristics will only lead to even stronger smoothing of precipitation in this region and to a decrease in average luminosity values.

In the final stage of the substorm growth phase (Fig. 5 *b*), the average emission intensity values increase by approximately 2 times compared to the quiet period (Fig. 5 *a*), and the area of maximum emission approaches *b* 2 *i* .

After the onset of the substorm expansion phase (Fig. 5 *c*), a narrow, well-defined peak of electron precipitation is recorded at the boundary of *b* 2 *i* , associated with a bright auroral arc with an average brightness in the green line $I_{557.7} \sim 30$ kR. The position of the brightest auroral arc immediately after the onset of the substorm expansion phase at the ion pressure maximum apparently indicates that the auroral breakup begins in the region of maximum ion pressure.

The lack of measurements of the pitch-angle distribution does not allow for an accurate identification of the nature of auroral precipitations at the precipitation peak, leading to the third brightness class of auroral emissions. One can only assume that a narrowly directed beam of electrons of ionospheric origin forms, similar to the type described in [Mende et al., 2003]. Within the framework of the substorm theory developed in [Antonova et al., 2002; Stepanova et al., 2002], such a beam is formed as a result of cold electrons of ionospheric origin penetrating into the region of longitudinal potential drop. Such penetration occurs as a result of a sharp increase in the plasma flow component across the pre-breakup arc before the moment T_0.

5. PROJECTIONS OF THE ISOTROPIZATION BOUNDARY IN THE EQUATORIAL PLANE OF THE MAGNETOSPHERE

As mentioned above, in isotropic plasma under conditions of magnetostatic equilibrium, the plasma pressure remains constant along the entire magnetic field line, excluding regions of longitudinal electron acceleration. This opens up the possibility to use the condition of equality of ion pressure, obtained from low-altitude satellite data, and measurements of ion pressure in the

equatorial plane of the magnetosphere to project ionospheric data into the equatorial plane without referring to any geomagnetic field models. The position of *b* 2 *i* in the ionosphere is close to the position of the maximum ion pressure, and its latitude indicates the most equatorial part of the ionosphere, the ion pressure of which can be projected into the equatorial magnetosphere.

To determine the radial distribution of ion pressure in the magnetosphere, observations from THEMIS mission satellites were used. The first results in this direction were obtained in the work [Kirpichev and Antonova, 2011]. Subsequently, such results were published in a number of works across the entire THEMIS database. The radial pressure distribution in the equatorial plane ($Z_{SM} = 0 \pm 1$ Re) in the 21:00-24:00 MLT sector is shown in Fig. 6. The ion pressure profile in Fig. 6 *a* was obtained for magnetically quiet conditions ($AL > -200$ nT, $Dst > -20$ nT, $Psw = 2.5 \pm 1.0$ nPa, Bz IMF $= 2.0 \pm 1.0$ nT), which approximately correspond to the conditions under which the latitudinal profile of ion pressure in the ionosphere shown in Fig. 4 *a* was obtained.

Fig. 6.

Fig. 6 *b* shows the ion pressure profile under quiet conditions, but with negative values of the Bz -component of the IMF ($AL > -200$ nT, $Dst > -20$ nT, $Psw = 3.5 \pm 1.0$ nPa, Bz IMF $= -1.0 \pm 1.0$ nT). Such parameters are closest to the substorm initiation phase and to the conditions corresponding to the ion pressure distribution in Fig. 4 *b* .

The data illustrated in Fig. 4 *a* , 4 *b* and Fig. 6 *a* , 6 *b,* allow for comparison of the latitudinal profile of ion pressure obtained at ionospheric altitudes with the radial distribution of ion pressure in Earth's magnetosphere. Under the condition of pressure equality along geomagnetic field lines, this makes it possible to determine the position of *b* 2 *i* and the entire ion pressure profile in the equatorial plane of the magnetosphere. The pressure comparison procedure can be briefly described as follows. The position of the pressure peak in the ionosphere is aligned with a point in the magnetosphere having an equal pressure value, and is fixed here. Then, linear scaling of the ionospheric pressure profile curve is performed until its best agreement with the magnetospheric pressure profile curve is achieved.

The results of such morphological projection (thin solid curve) and comparison with the radial pressure profile according to THEMIS data (curve with dots) are presented in Fig. 7. The upper horizontal scale in Fig. 7 shows corrected geomagnetic latitudes, and the lower one shows the radial distance to which these latitudes are projected onto the equatorial plane of the magnetosphere. Since the scatter of data in the equatorial plane at large Re is very significant, the upper and lower scales in this representation are not interpreted as corresponding to each other along the entire length. The important aspects of this approach are (1) the similarity of ion pressure behavior with increasing

latitude in the ionosphere and distance in the equatorial plane when determined only at two extreme points: the position of the maximum at ionospheric heights and the position of minimum pressure at distances of ~13−14 Re, and (2) determining the projection position of the boundary *b* 2 *i* in the equatorial plane.

Fig. 7.

The position of the boundary *b* 2 *i* is marked with dashed lines in Fig. 7. Figure 7 (upper panel) shows that under quiet conditions with low magnetic activity and positive values of the vertical component of the IMF, *b* 2 *i* projects to the equatorial plane at distances of ~7.5 Re. Figure 7 (lower panel) shows a comparison of pressure profiles in the equatorial plane and at ionospheric heights during the final stage of the substorm growth phase. This figure indicates that compared to the quiet period, during the substorm growth phase, *b* 2 *i* shifts toward the equator and is recorded at a distance of ~5.2 Re before the onset of the substorm expansion phase. The segment of the bold dashed line on the lower horizontal scale of Fig. 7 *a* and Fig. 7 *b* shows the distance interval corresponding to the root-mean-square error in calculating the mean ion pressure.

During the substorm expansion phase, due to the presence of various mechanisms of enhancement and weakening of precipitating particle fluxes and high levels of turbulent fluctuations, the morphological projection method can no longer be used. Based on the fact that the latitudinal position of *b* 2 *i* in the final stage of the substorm growth phase and at the beginning of the expansion phase remains unchanged, and taking into account the appearance of an area of strong local electron precipitation near *b* 2 *i* , it can be concluded that the auroral breakup in the pre-midnight sector of the magnetosphere is on average recorded at distances of ~5-6 Re from Earth.

6. DISCUSSION AND RESULTS

Observations from the F7 satellite in the 21:00-24:00 MLT sector were used to determine the average characteristics of precipitating electrons and ions. The average latitudinal profiles of ion pressure and auroral luminosity at ionospheric altitudes during quiet periods and during the onset of magnetospheric substorms were obtained. To determine the average radial distribution of ion pressure in the equatorial plane of the magnetosphere, observations from the THEMIS mission satellites were used. Comparison of the latitudinal distribution of plasma pressure at ionospheric altitudes with plasma pressure in the equatorial plane made it possible to significantly clarify the localization of the onset region of the explosive phase of a classical substorm in Earth's magnetosphere without using any geomagnetic field model.

The main results of the study can be formulated as follows .

1. Average latitudinal profiles of ion pressure in the pre-midnight sector were obtained, calculated from measurements of the F7 satellite, under magnetically quiet conditions, in the final period of the growth phase, and in the initial period of the expansion phase of substorms.
2. It is shown that the maximum in the latitudinal pressure profile closely coincides with the position of the ion precipitation boundary *b* 2 *i* according to the classification of [Newell et al., 1998]. The latitude of the *b2i* boundary during quiet periods is $\Phi' = 68.3° \pm 0.6°$ CGL, while before the onset of a substorm and in the initial period of its expansion phase, the *b* 2 *i* boundary is located at latitudes $\Phi' = 65.4° \pm 0.7°$ CGL.
3. Based on THEMIS satellites observations, average radial profiles of plasma pressure were obtained in the pre-midnight sector during magnetically quiet conditions (*AL* >−200 nT, *Bz* IMF>0) and during periods most closely corresponding to the substorm growth phase in terms of interplanetary medium parameters and geomagnetic activity level (*AL* > − 200 nT, but *Bz* IMF<0).
4. Comparison of ion pressure in the ionosphere and pressure in the equatorial plane indicates that under magnetically quiet conditions the boundary *b* 2 *i* projects to a geocentric distance of ~7.5 Re. Compared to the quiet period, during the substorm growth phase, the *b* 2 *i* boundary shifts earthward to closer distances of 5−6 Re.
5. Assessments of auroral luminosity brightness in the 557.7 nm emission were carried out, calculated from observations of the average energy and energy flux of precipitating electrons by the F7 satellite. It is shown that during quiet periods and before the onset of a substorm, aurora are recorded in the region of isotropic precipitation poleward of the *b* 2 *i* boundary.
6. In the initial period of the substorm expansion phase, the existence of a local, narrow, clearly defined peak of electron precipitation at the *b* 2 *i* boundary has been statistically demonstrated, associated with a bright auroral arc with an intensity in the green line of $I_{557.7} \sim 30$ kR.

The position of the brightest auroral arc after the beginning of the substorm expansion phase at the *b* 2 *i* boundary apparently indicates that the auroral breakup begins in the region of maximum ion pressure at ionospheric heights. The results obtained in this work give reason to assume that the auroral breakup area projects into the Earth's magnetosphere at geocentric distances of ~5−6 Re.

The movement of the equatorial boundary of the auroral oval to lower latitudes with the beginning of the substorm growth phase was discovered in the 1970s. The shift of the *b* 2 *i* boundary toward the equator during the stretching of magnetic field lines into the magnetospheric tail was

noted in the work of (Newell et al., 1998) and was considered as a result of the dynamics of the magnetospheric tail current. However, comparisons of statistically obtained pressure values at low altitudes and near the equatorial plane, taking into account the position of the boundary *b* 2 *i* have not been conducted to date. As a result of the research performed in this work, it was possible to determine the magnitude of the *b* 2 *i* shift during the transition from magnetically quiet conditions (~7.5 Re) to the beginning of the substorm development phase (5−6 Re). The existence of such a shift indicates the localization of the onset of the explosive phase of the substorm deep within the ring current and may support the assertion that there are no qualitative differences in the development mechanisms between isolated substorms and substorms during a magnetic storm. However, verification of the latter statement requires additional research.

It is also necessary to discuss the approach of Newell et al. [1998], in which the stretching of magnetic field lines is associated with the development of currents in the magnetospheric tail. Analysis of THEMIS mission data allowed for the identification of a plasma region surrounding the Earth with characteristics corresponding to the "near-Earth plasma sheet region" and the identification of a plasma ring surrounding the Earth [Antonova et al., 2013, 2014]. It was shown that the averaged radial gradient of plasma pressure in the ring is directed toward the Earth, indicating the presence of an outer ring current region. Such current is concentrated near the equator only in the evening, night, and morning hours, while during daytime hours, due to compression of the magnetosphere by the solar wind and the shift of magnetic field minima to high latitudes, it is spread along the magnetic field line (see review [Antonova et al., 2018]). The outer boundary of this current region is localized at geocentric distances of ~10-13 Re, which significantly exceeds the geocentric distance of the projection *b* 2 *i* onto the equatorial plane. With the development of the ring current in regions where plasma pressure becomes comparable to magnetic field pressure, magnetic field lines are stretched in the radial direction and a magnetic disk is formed. Such a structure appeared in Earth's magnetosphere modeling starting with the T-89 model [Tsyganenko, 1989]. The stretching of magnetic field lines observed during the preliminary phase of a substorm at geostationary orbit is most likely mainly associated with the development of the ring current, including its outer part. The observed dipolarizations within the ring current can be associated with the development of plasma distribution instability and large-scale field-aligned currents, which allows us to not consider processes in the turbulent magnetospheric tail as a mandatory mechanism for substorm disturbances.

The brightening observed at the beginning of the explosive phase of a substorm in the auroral arc closest to the equator, of the third and, in some cases, the fourth brightness class, fits well into

the above-described scheme of substorm processes. Such brightening corresponds to the formation of a beam of ionospheric electrons that are cold in the transverse direction, penetrating into the region of longitudinal potential drop. The density of cold electrons of ionospheric origin at the heights of the longitudinal acceleration region (~10−10 ^{2} cm $^{-3}$) exceeds the density of magnetospheric electrons by one to two orders of magnitude, which leads to the appearance of third and fourth brightness class emissions. The scenario described above differs significantly from the generally accepted ones. Therefore, much remains to be done to verify the picture of substorm process development described above.

ACKNOWLEDGEMENTS

The authors thank the teams of the DMSP and THEMIS projects for the opportunity to use the data published on the websites (https://themis.ssl.berkeley.edu/data/themis/) and (https://dmsp/bc/edu/). IMF parameters, solar wind plasma parameters, and magnetic activity indices were taken from the pages (http://cdaweb.gsfc.nasa.gov/) and (http://wdc.kugi.kyoto-u.ac.jp/) .

FUNDING

The research performed by Vorobyev V.G. was supported by the Russian Science Foundation (RSF), project 22-12-20017.

REFERENCES

- *Vorobyev V.G., Kirillov A.S., Katkalov Yu.V., Yagodkina O.I.* Planetary distribution of auroral emission intensity obtained using the auroral precipitation model // Geomagnetism and Aeronomy. Vol. 53. No. 6. P. 757−761. 2013. https://doi.org/10.7868/S0016794013060163
- *Despirak I.V., Kleimenova N.G., Lyubchich A.A., Malysheva L.M., Gromova L.I., Roldugin A.V., Kozelov B.V.* Magnetic substorms and aurora at polar latitudes of Spitsbergen: Event of December 17, 2012. Izv. RAN. Ser. Physical. Vol. 86. No. 3. P. 340−348. 2022. https://doi.org/ 10.31857/S0367676522030097
- *Kirpichev I.P., Antonova E.E.* Plasma pressure distribution in the equatorial plane of the Earth's magnetosphere at geocentric distances from 6 to 10 R_E according to the international project THEMIS data // Geomagnetism and Aeronomy. Vol. 51. No. 4. P. 456−461. 2011.

− *Kleimenova N.G., Antonova E.E., Kozyreva O.V., Malysheva L.M., Kornilova T.A., Kornilov I.A.* Wave structure of magnetic substorms at polar latitudes // Geomagnetism and Aeronomy. Vol. 52. No. 6. P. 785–793. 2012.

− *Akasofu S.-I.* The development of the auroral substorm // Planet. Space Sci. V. 12. N 4. P. 273−282. 1964. https://doi.org/10.1016/0032-0633(64)90151-5

– *Antonova E.E* . The results of INTERBALL/Tail observations, the inner magnetosphere substorm onset and particle acceleration // Adv. Space Res. V. 30. N 7. P. 1671−1676. 2002. https://doi.org/10.1016/S0273-1177(02)00434-9

– *Antonova E.E., Kirpichev I.P., Vovchenko V.V., Stepanova M.V., Riazantseva M.O., Pulinets M.S., Ovchinnikov I.L., Znatkova S.S. C* haracteristics of plasma ring, surrounding the Earth at geocentric distances ~7-10 R_E, and magnetospheric current systems // J. Atmos. Sol.-Terr. Phy. V. 99. P. 85–91. 2013. https://doi.org/10.1016/j.jastp.2012.08.013

– *Antonova E.E., Kirpichev I.P., Stepanova M.V.* Plasma pressure distribution in the surrounding the Earth plasma ring and its role in the magnetospheric dynamics // J. Atmos. Sol.-Terr. Phy. V. 115–116. P. 32–40. 2014. https://doi.org/10.1016/j.jastp.2013.12.005

– *Antonova E.E., Stepanova M., Kirpichev I.P., Ovchinnikov I.L, et al.* Structure of magnetospheric current systems and mapping of high latitude magnetospheric regions to the ionosphere // J. Atmos. Sol.-Terr. Phy. V. 177. P. 103–114. 2018. https://doi.org/10.1016/j.jastp.2017.10.013

– *Baker K.B., Wing S.* A new magnetic coordinate system for conjugate studies at high latitudes // J. Geophys. Res. – Space. V. 94. N 7. P. 9139–9144. 1989. https://doi.org/10.1029/JA094iA07p09139

– *Baker D.N., Pulkkinen T.I., Angelopoulos V., Baumjohann W., McPherron R.L.* Neutral line model of substorms: Past results and present view // J. Geophys. Res. – Space. V. 101. N 6. P. 12975−13010. 1996. https://doi.org/10.1029/95JA03753

– *Dubyagin S.V., Sergeev V.A., Carlson C.W., Marple S.R., Pulkkinen T.I., Yahnin A.G.* Evidence of near-Earth breakup location // Geophys. Res. Lett. V. 30. N 6. ID 1282. 2003. https://doi.org/10.1029/2002GL016569

−*Goertz C.K., Baumjohann W.* On the thermodynamics of the plasma sheet // J. Geophys. Res. – Space. V. 96. N 12. P. 20991–20998. 1991. https://doi.org/10.1029/91JA02128

− *Kim H.-J., Kim K.-C., Noh S.-J., Lyons L., Lee D.-Y., Choe W.* New perspective on phase space density analysis for outer radiation belt enhancements: The influence of MeV electron injections // Geophys. Res. Lett. V. 50. N 14. ID e2023GL104614. 2023. https://doi.org/10.1029/2023GL104614

− *Kirpichev I.P., Antonova E.E., Stepanova M., Eyelade A.V., Espinoza C.M., Ovchinnikov I.L.,Vorobjev V. G., Yagodkina O.I.* Ion kappa distribution parameters in the magnetosphere of the Earth at geocentric distances smaller than 20 R_E during quiet geomagnetic conditions // J. Geophys. Res. – Space. V. 126. N 10. ID e2021JA029409. 2021. https://doi.org/10.1029/2021JA029409

– *Lui A.T.Y.* Current disruption in the Earth's magnetosphere: Observations and models // J. Geophys. Res. – Space. V. 101. N 6. P. 13067−13088. 1996. https://doi.org/10.1029/96JA00079

– *Mende S.B., Carlson C.W., Frey H.U., Peticolas L.M., Østgaard N.* FAST and IMAGE-FUV observations of a substorm onset // J. Geophys. Res. – Space. V. 108. N 9. ID 1344. 2003. https://doi.org/10.1029/2002JA009787

− *Newell P.T., Feldstein Ya.I., Galperin Y.I., Meng S.-I.* The morphology of nightside precipitation // J. Geophys. Res. – Space. V. 101. N 5. P. 10737−10748. 1996. https://doi.org/10.1029/95JA03516

− *Newell P.T., Sergeev V.A., Bikkuzina G.R., Wing S.* Characterizing the state of the magnetosphere: Testing the ion precipitation maxima latitude (b 2 i) and the ion isotropy boundary // J. Geophys. Res. – Space. V. 103. N 3. P. 4739−4745. 1998. https://doi.org/10.1029/97JA03622

− *Nosé M., Keika K., Kletzing C.A., Spence H.E., Smith C.W., MacDowall R.J., Reeves G.D.* , *Larsen B.A., Mitchell D.G.* Van Allen Probes observations of magnetic field dipolarization and its associated O^+ flux variations in the inner magnetosphere at $L < 6.6$ // J. Geophys. Res. – Space. V. 121. N 8. P. 7572–7589. 2016. https://doi.org/10.1002/2016JA022549

− *Nosé M., Matsuoka A., Kasahara S., et al.* Magnetic field depolarization and its associated ion flux variations in the dawnside deep inner magnetosphere: Arase observations // Geophys. Res. Lett. V. 45. N. 16. P. 7942–7950. 2018. https://doi.org/10.1029/2018GL078825

− *Persson M.A.L., Opgenoorth H.J., Pulkkinen T.I., et al.* Near-earth substorm onset: A coordinated study // Geophys. Res. Lett. V. 21. N. 17. P. 1875−1878. 1994. https://doi.org/10.1029/94GL01426

– *Paschmann G., Haaland S., Treumann R.* Auroral plasma physics // Space Sci. Rev. V. 103. N 1–4. P. 1–485. 2002. https://doi.org/10.1023/A:1023030716698

– *Roach F.E., Jamnick P.M.* The sky and eye // Sky and Telescope. V. 17. P. 164–168. 1958.

− *Stepanova* M.V., *Antonova E.E., Bosqued J.M., Kovrazhkin R.A., Aubel K.R.* Asymmetry of auroral electron precipitations and its relationship to the substorm expansion phase onset // J. Geophys. Res . – Space. V. 107. N 7. ID 1134. 2002. https://doi.org/10.1029/2001JA003503

− *Stepanova M., Antonova E.E., Bosqued J.-M.* Study of plasma pressure distribution in the inner magnetosphere using low-altitude satellites and its importance for the large-scale magnetospheric dynamics // Adv. Space Res. V.38. N 8. P.1631−1636. 2006. https://doi.org/10.1016/j.asr.2006.05.013

– *Tsyganenko N.A.* A magnetospheric magnetic field model with a warped tail current sheet // Planet. Space Sci. V. 37. N 1. P. 5 − 20. 1989. https://doi.org/10.1016/0032-0633(89)90066-4

– *Vorobjev V.G., Yagodkina O.I., Starkov G.V., Feldstein Ya. I.* A substorm in midnight auroral precipitation // Ann. Geophys. V. 21. N. 12. P. 2271–2280. 2003. https://doi.org/10.5194/angeo-21-2271-2003

– *Vorobjev V.G., Antonova E.E., Yagodkina O.I.* How the intensity of isolated substorms is controlled by the solar wind parameters // Earth Planets Space. V. 70. N 1. ID 148. 2018. https://doi.org/10.1186/s40623-018-0922-5

– *Vorobjev V.G., Yagodkina O.I., Antonova E.E.* Ionospheric features of polar cusp dayside precipitation under a northern IMF // Geomagn. Aeronomy. V. 64. N 3. P. 302–312. 2024. https://doi.org/10.1134/S0016793224600103

− *Wing S., Newell P.T.* Center plasma sheet ion properties as inferred from ionospheric observations // J. Geophys. Res. – Space. V. 103. N. A4. P. 6785−6800. 1998. https://doi.org/ 10.1029/97JA02994

Figure captions

Fig. 1. Variations of interplanetary medium parameters and geomagnetic activity levels on October 8, 1986, in the interval 01:00-05:00 UT. From top to bottom: variations of the *Bz* component of the IMF and solar wind dynamic pressure, variations of *AL* -, *SYM/H* - and *PC indices* of magnetic activity. IMF and solar wind data are recalculated to the subsolar point of the shock front. The time of the F7 satellite passage is indicated by a vertical dashed line.

Fig. 2. Integral characteristics of precipitating particles observed by the F7 satellite on October 8, 1986, at 03:09-03:10 UT: (*a)*− average energies (*Ei* , keV) and energy fluxes (*Fi* , erg/cm ^{2} s) of precipitating ions, (*b*) – average energies (*Ee* , keV) and energy fluxes (*Fe* , erg/cm ^{2} s) of precipitating electrons. The horizontal axis shows the corrected geomagnetic latitude (CGL). Horizontal dashed lines indicate the position of the boundary *b* 2 *i* .

Fig. 3. Latitudinal profiles of ion pressure (*a*) and emission intensity at 557.7 nm (*b*), calculated from the data in Fig. 2 *a* and 2 *b* respectively. Vertical dashed lines indicate the position of the boundary *b* 2 *i* .

Fig. 4. Average latitudinal profiles of ion pressure, *Pi* (nPa): (*a*) – magnetically quiet period, (*b*) – final stage of the substorm growth phase, (*c*) – initial stage of the substorm expansion phase. Vertical dashed lines indicate the average position of *b* 2 *i* .

Fig. 5. Average latitudinal profiles of emission intensity at 557.7 nm, I_{5577} (kR). Panels (*a*−*c*) correspond to panels (*a*−*c*) in Fig. 4. Vertical dashed lines indicate the average position of *b* 2 *i* .

Fig. 6. Radial distribution of ion pressure in the pre-midnight sector of the Earth's magnetosphere during magnetically quiet periods with positive (*a*) and negative (*b*) polarity of the vertical IMF component.

Fig. 7. Projection of the latitudinal profile of ion pressure in the ionosphere onto the equatorial plane of the magnetosphere (thin curve) and its comparison with observations in the equatorial plane (curve with points). Upper panel – magnetically quiet period; lower panel – final stage of the substorm growth phase.

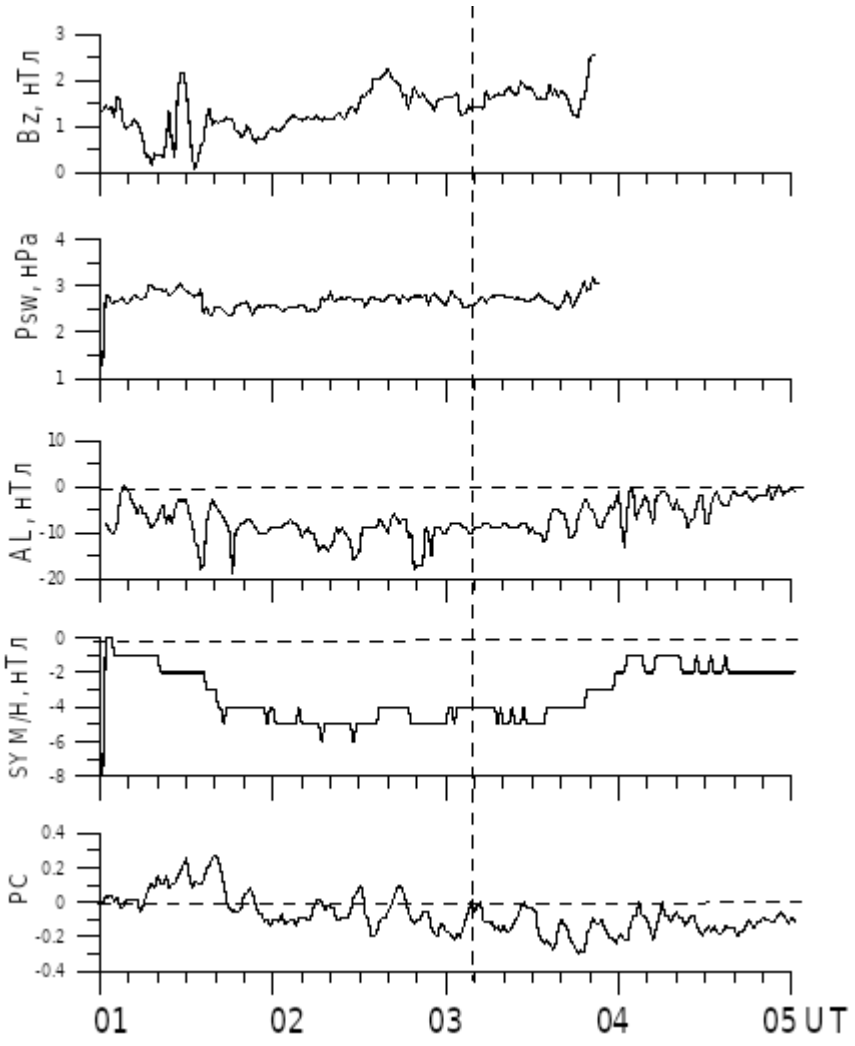
Bz, нТл
3
2
1
0
Psw, нРа
4
3
2
1
AL, нТл
10
0
-10
-20
SYM/H, нТл
0
-2
-4
-6
-8
PC
0.4
0.2
0
-0.2
-0.4
01
02
03
04
05 UT

Fig. 1.

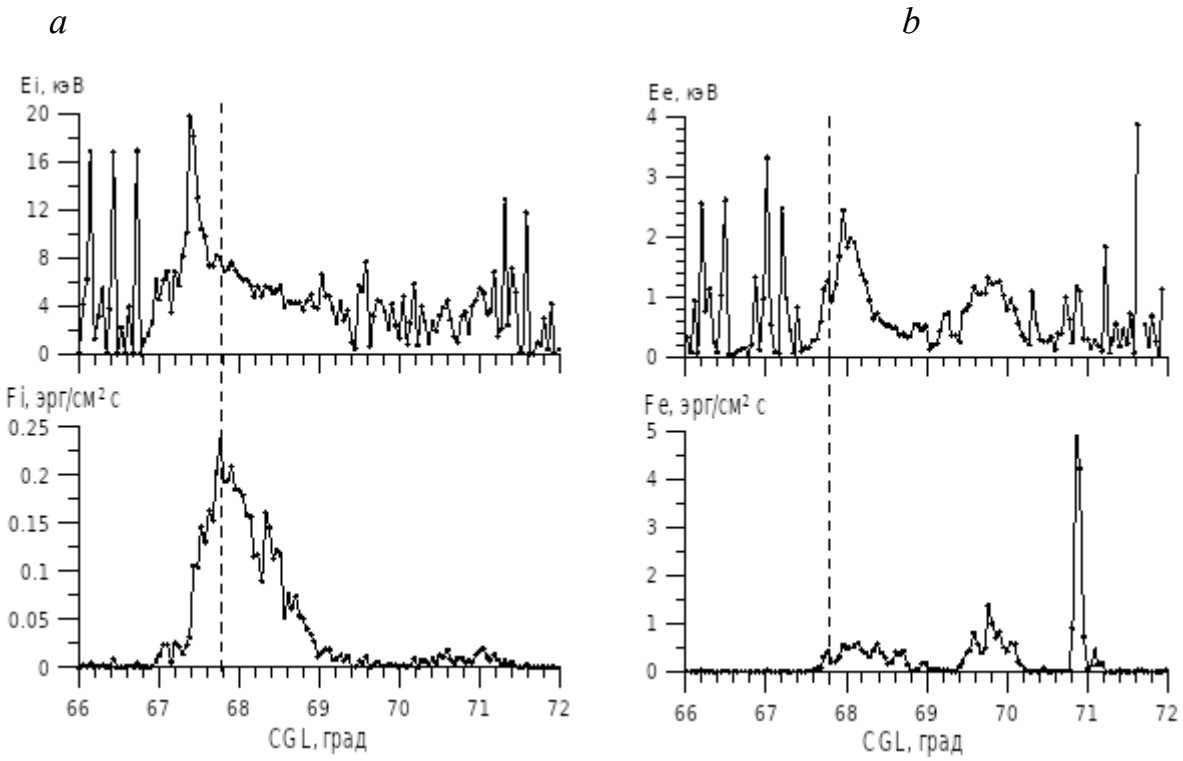
a
b
Ei, кэВ
Ee, кэВ
Fi, эрг/см² с
Fe, эрг/см² с
CGL, град
CGL, град

Fig. 2.

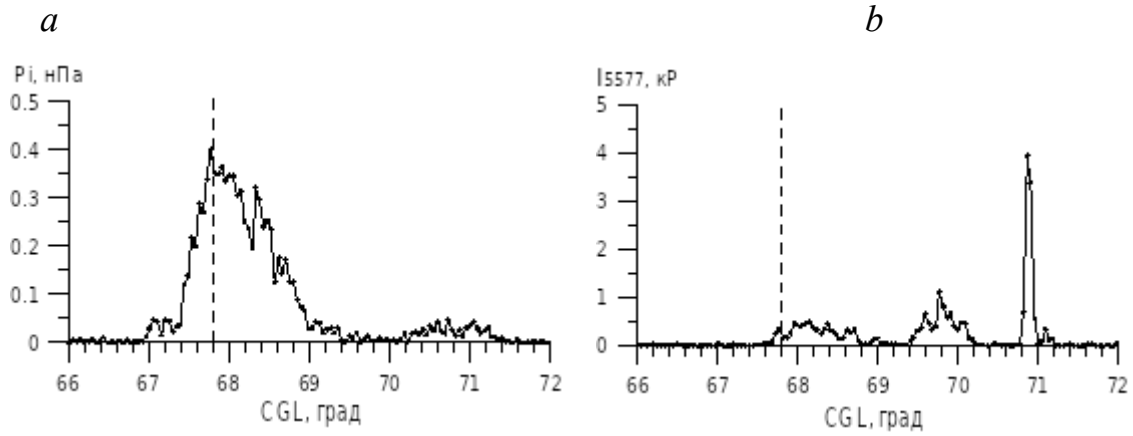
a
b
Pi, нПа
I5577, кР
CGL, град
CGL, град

Fig. 3.

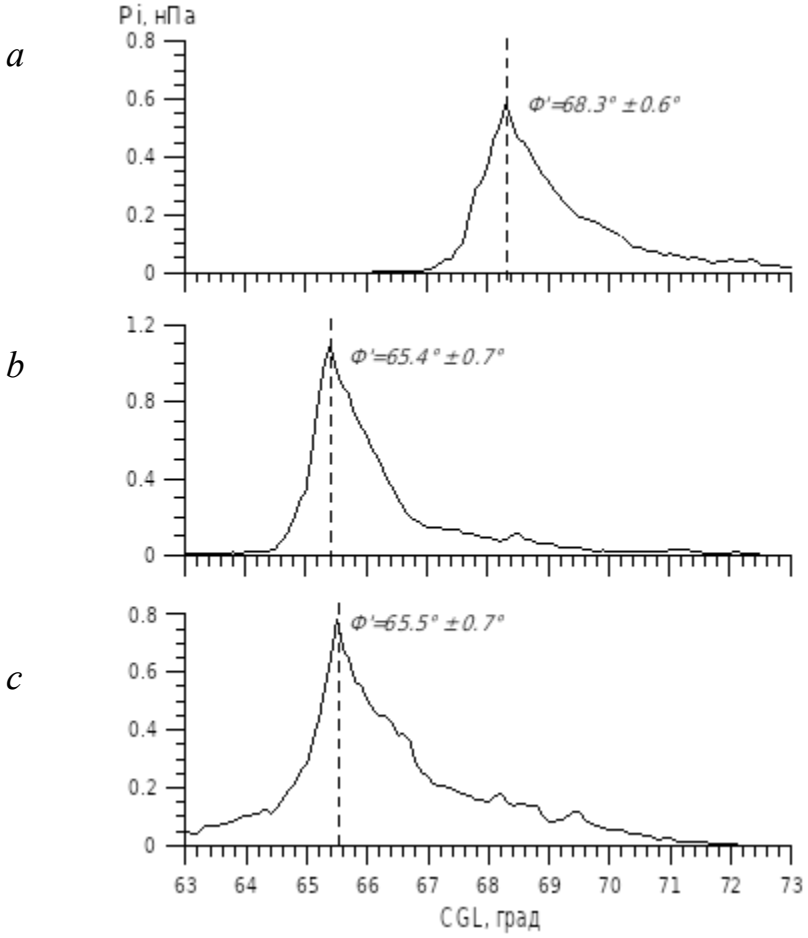
Pi, нПа
a
0.8
0.6
0.4
0.2
0
Φ'=68.3° ± 0.6°
b
1.2
0.8
0.4
0
Φ'=65.4° ± 0.7°
c
0.8
0.6
0.4
0.2
0
Φ'=65.5° ± 0.7°
63
64
65
66
67
68
69
70
71
72
73
CGL, град

Fig. 4.

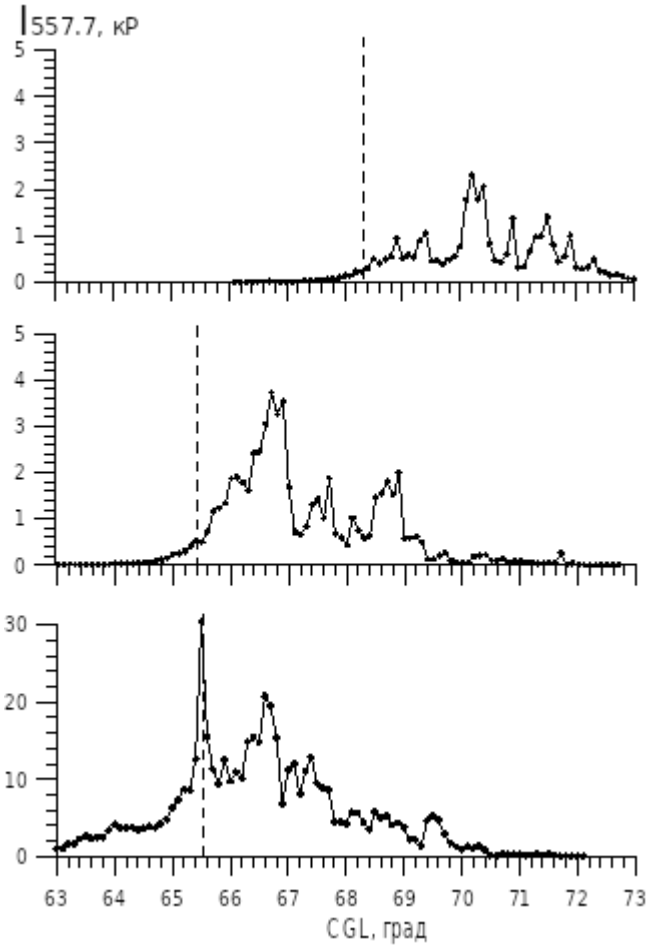
557.7, кР
5
4
3
2
1
0
5
4
3
2
1
0
30
20
10
0
63
64
65
66
67
68
69
70
71
72
73
CGL, град

a

b

c

Fig. 5

a

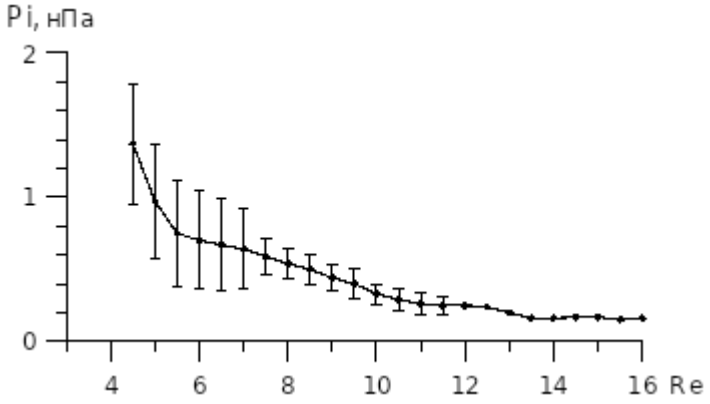

b

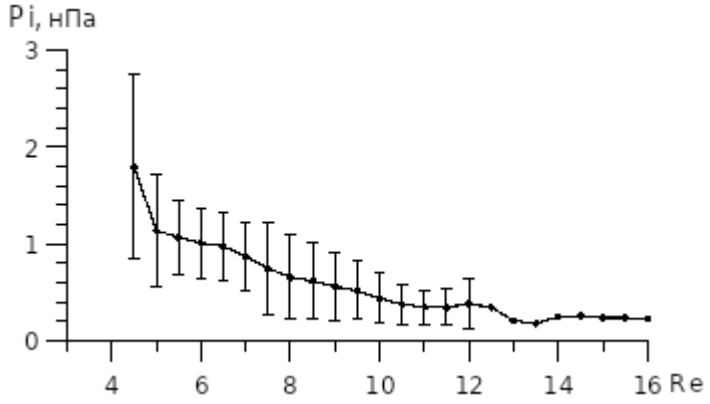

Fig. 6.

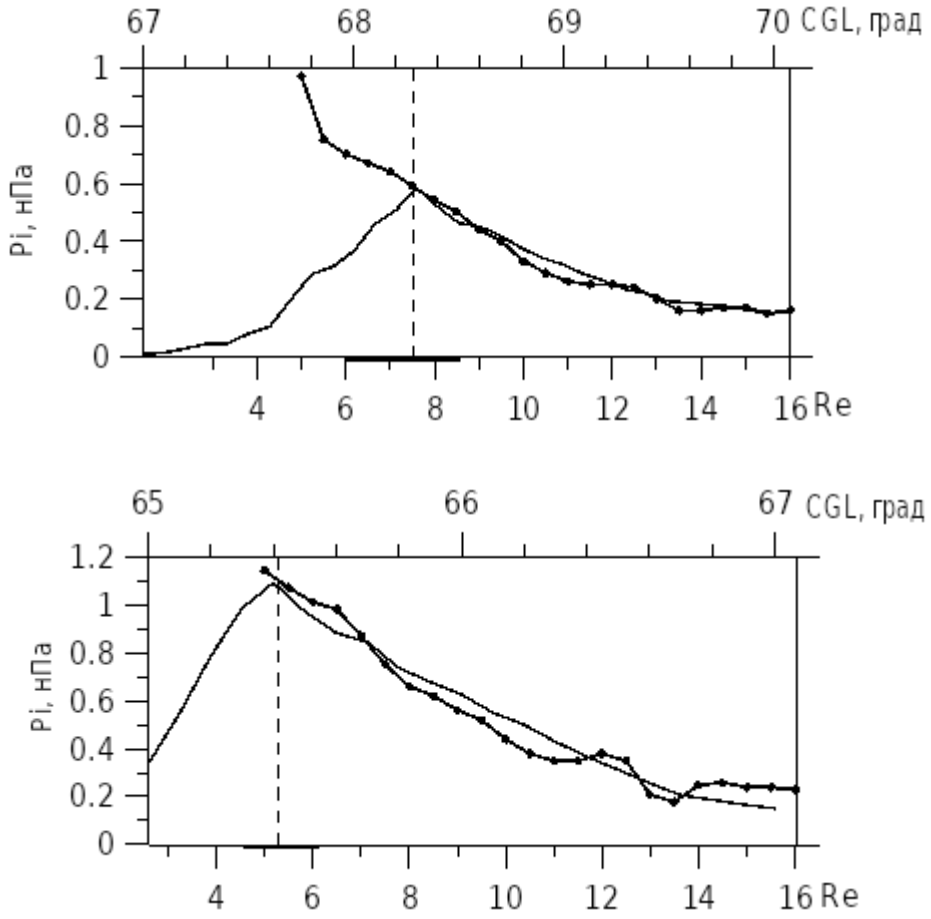
67
68
69
70 CGL, град
1
0.8
0.6
0.4
0.2
0
Pi, нПа
4
6
8
10
12
14
16 Re
65
66
67 CGL, град
1.2
1
0.8
0.6
0.4
0.2
0
Pi, нПа
4
6
8
10
12
14
16 Re

Fig. 7.